SUPPLEMENT TO THE *WELDING JOURNAL,* JUNE 2011
Sponsored by the American Welding Society and the Welding Research Council

Measuring Welding Deformations with the Digital Image Correlation Technique

Digital image correlation does not have some of the drawbacks for measuring deformation during welding as more commonly used methods

BY M. DE STRYCKER, P. LAVA, W. VAN PAEPEGEM, L. SCHUEREMANS, AND D. DEBRUYNE

ABSTRACT

The finite element simulation of a welding process is usually validated by temperature evolution, microstructure analysis, residual stress measurement, or strain evolution. Several methods are available for measuring the strain evolution, and in this research, we investigate if the digital image correlation (DIC) technique can record the strain evolution during welding. Compared to other measuring methods used in welded structures, DIC has the major advantages that it is a contactless method, and it can give the strain evolution over a significant portion of the surface when a workpiece is welded, even in zones where temperature reaches 600°C, without the need for thermal compensation on the measured strains. The case investigated was a stainless steel tube with a longitudinal weld bead on top. It was shown that if enough images were taken, the strain evolution was in agreement with that found by electrical strain gauges.

Introduction

Welding simulations are usually split up into two separate analyses: First, the thermal field evolution in the welded construction is calculated from the heat input and next, starting from the temperature field, the stress and strain development due to the welding is calculated in a mechanical analysis. As the finite element (FE) simulation is split up, the validation can be done on the two fields: either the temperatures or the stress/strain development can be checked, or both. The thermal field used for the mechanical simulation can be validated by measuring the transient temperatures or the resulting microstructure in the welded construction (Ref. 1). Since the thermal simulation comprises a select set of material properties and measuring temperatures is not too difficult, it is less complicated to establish the thermal field. In the mechanical analysis, more material parameters are introduced and more assumptions are made, inducing a more complicated stress/strain validation. Lindgren (Ref. 1) gives an extensive overview of papers describing validation methods for the mechanical analysis. These include residual stress measurements using hole-drilling techniques, X-ray techniques, or neutron diffraction measurements. Transient strains have also been measured in some cases using high-temperature strain gauges.

Muramatsu et al. (Ref. 2) reported the measuring of strain evolution during a welding operation with a laser speckle method. They concluded that with that method, it is possible to perform strain measurements just after weld metal solidification in gas tungsten arc (GTA) welding of thin SUS304 steel sheets and considered this as an enhancement of the numerical calculation strategy. They reported a method to effectively shield the arc light and the disturbance effect of heating-induced convection. Mikami et al. (Ref. 3) measured the vertical displacements of 9 points on skin-plates in a T-joint by laser displacement sensors. From these, the angular distortions are calculated. Schwenk et al. (Ref. 4) recorded the transient longitudinal and transverse distortions with seven displacement transducers during a bead-on-plate laser weld on a dual-phase steel. Synchrotron X-ray diffraction residual stress measurements were used by Van der Aa et al. (Refs. 5, 6) for validation of a bead-on-plate GTA weld on flat DP600 samples. Courtin et al. (Ref. 7) used the center hole drilling method to retrieve the residual stresses in a multipass weld between a ferritic and an austenitic steel pipe.

The mentioned methods have some drawbacks: Only in a restricted number of points for the deformations and strains are available (in the case of displacement sensors, strain gauges), temperature compensation is needed (for strain gauges), only the final stress/strain state is known (for residual stress measurements), the part is damaged (destructive residual stress measuring methods), the method requires a complex setup (laser interferometry, X-ray diffraction, and neutron diffraction residual stress measurements), there is sensitivity to vibrations, and there are differences in the density of the air between the measurement device and the welded object (laser interferometry).

An alternative method, which counters some of these drawbacks, and to the authors' knowledge, has not yet been used for measuring deformations during welding, is digital image correlation (DIC). The DIC method has a simple setup compared to other measuring methods, is insensitive to rigid body motions (vibrations), does

M. DE STRYCKER (maarten.destrycker@kahosl.be) *and P. LAVA are with MeM2P research group, Catholic University College Ghent, Ghent, Belgium. W. VAN PAEPEGEM is with Department of Materials Science and Engineering, Ghent University, Ghent, Belgium. L. SCHUEREMANS is with Department of Civil Engineering, KULeuven, Heverlee, Belgium. D. DEBRUYNE is with Department MTM, KULeuven, Heverlee, Belgium.*

KEYWORDS

GTAW
Cold-Rolled Steel Tubes
Digital Image Correlation
Electrical Strain Gauges
Thermal Strain

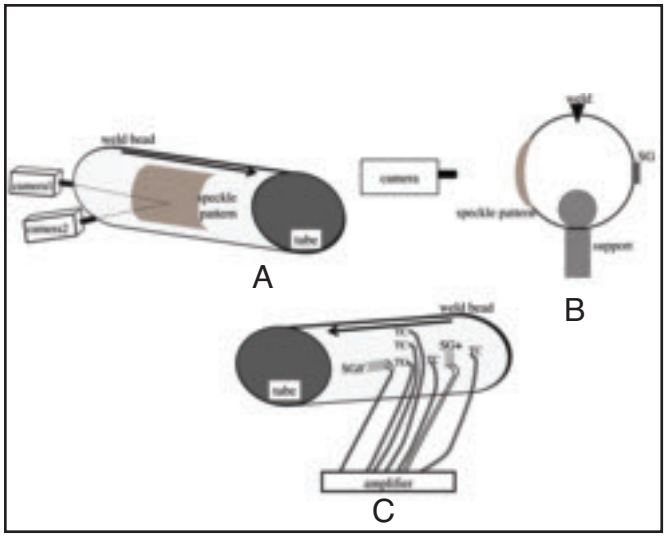

Fig. 1 — Sketch of the setup. The cameras film the speckle pattern and, symmetrical with regard to the weld bead, two strain gauges (SG+ in the hoop direction and SG// in the longitudinal direction) and thermocouples (TC) are applied to the tube. The bottom of the tube is clamped between a circular bar inside and a rectangular support outside.

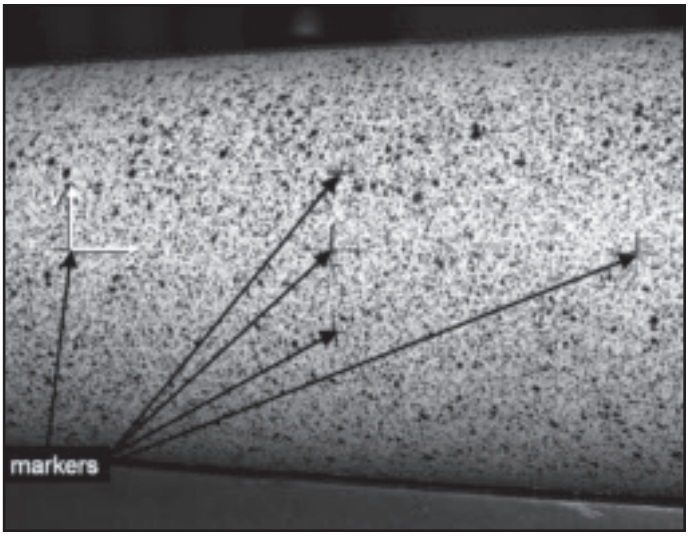

Fig. 2 — Typical speckle pattern for this setup. Black crosses are used as reference markers for the definition of the coordinate system: The x-axis is in a longitudinal direction of the tube, and the y-direction is in hoop direction.

not need temperature compensation, is contactless, and reveals the transient strain state over a wide surface of the welded object. It has, however, the drawback that it is conventionally not judged suited for small strains (below 1000 μm m^{-1}) that occur in the welding case under consideration here (Ref. 8). In this research, it is investigated whether it is possible to observe with sufficient accuracy the deformations during a welding process using DIC.

Thermal strains up to 650°C were already successfully measured with DIC by Lyons et al. (Ref. 9) and more recently on uniformly heated 3-D tubular specimens by the authors (Ref. 8), under the conditions that sufficient data are collected by taking enough images, that the strain is taken as the average over the homogeneous strain area, and putting the temperature limit to 600°C. Analogous conclusions with a limit to 550°C were taken by Pan et al. (Ref. 10).

As it was the first time that the DIC technique was used for measuring inhomogeneous thermal strain fields in the range below 1000 μm m^{-1}, the strain field measured with the DIC technique was compared with the strains obtained by electrical strain gauges (SG), put on the tube as a reference.

This research is part of a larger project in which the residual stresses in cold-rolled steel tubes due to the weld bead that closes the cross section are investigated. The real production process, where the steel plate is rolled into a circular cross section and passes underneath a GTAW torch, is in the laboratory setup, modified to a static setup in which the GTAW moves (slower than in the real process) over a finished tube.

Digital Image Correlation

As an optical full-field measurement method, DIC has turned out to be an ideal tool to identify the mechanical material behavior through inverse modeling (Refs. 11, 12) and to study the deformation characteristics of a wide range of materials (Refs. 13, 14). In the following, only a short introduction to the technique is given. More information can be found in Sutton et al. (Ref. 15).

The basic principle behind the technique is to calculate the displacements on the surface of an object by taking images of a black and white speckle pattern in the undeformed and the deformed state. As the speckle pattern is attached to the material underneath, the deformation of the speckle pattern is the same as the surface material of the object under investigation. To follow the strain evolution during a process, a lot of images can be made and the speckle pattern deformation in the series of images can be followed.

The gray-value images of the speckle pattern deformation are captured with a coupled charged device (CCD) camera. Since a 3-D object is undergoing spatial deformations, two cameras are needed for stereovision.

To reveal the deformations of the object during the experiment, typically a square subset of pixels (px) from the undeformed image is taken, and its location in the deformed image is traced. This subset may undergo various transformations between the different images. To be sure that the same subset of gray values is found in the deformed image, a correlation criterion is used to judge the accuracy of the match.

For a successful correlation, the speckle pattern should be random (i.e., have a unique subset in each image) and have a good black and white balance because from a complete black or complete white subset, no displacement information can be gathered. Therefore, the size of the subset is related to the size of the speckles: The subset size should be larger than the largest speckle.

In view of the smooth deformations in the application under investigation, the subset deformation is restricted to an affine transformation during the analysis. As the displacements from one image to the other may be smaller than one pixel, the subset in the deformed image is not likely to fit on the pixel grid and an interpolation method between the pixels is needed. Previous research (Refs. 16, 17) has shown that the normalized sum of squared difference (NSSD) correlation algorithm with cubic B-spline interpolation reduces the systematic errors in the correlation process. In this way, for every pixel in the undeformed image, the displacement in all the deformed images can be calculated. In practice, a certain step

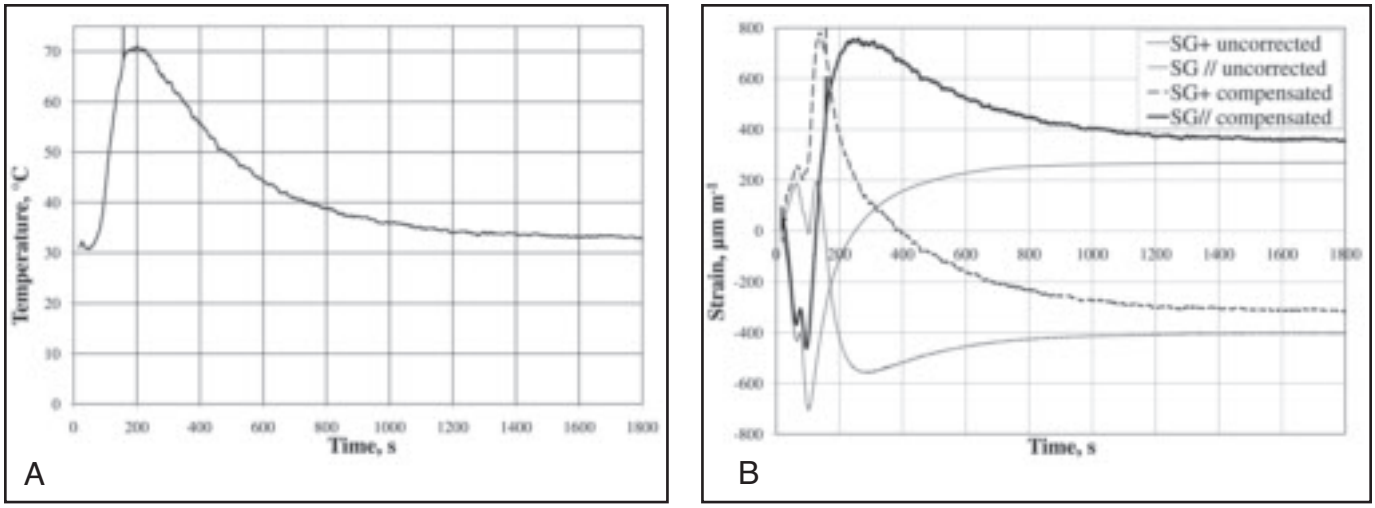

Fig. 3 — A — Temperature curve used for compensation; B — uncorrected and compensated strain evolution as observed with SG. SG+ is the strain gauge in the hoop direction and SG// is the SG in the longitudinal direction.

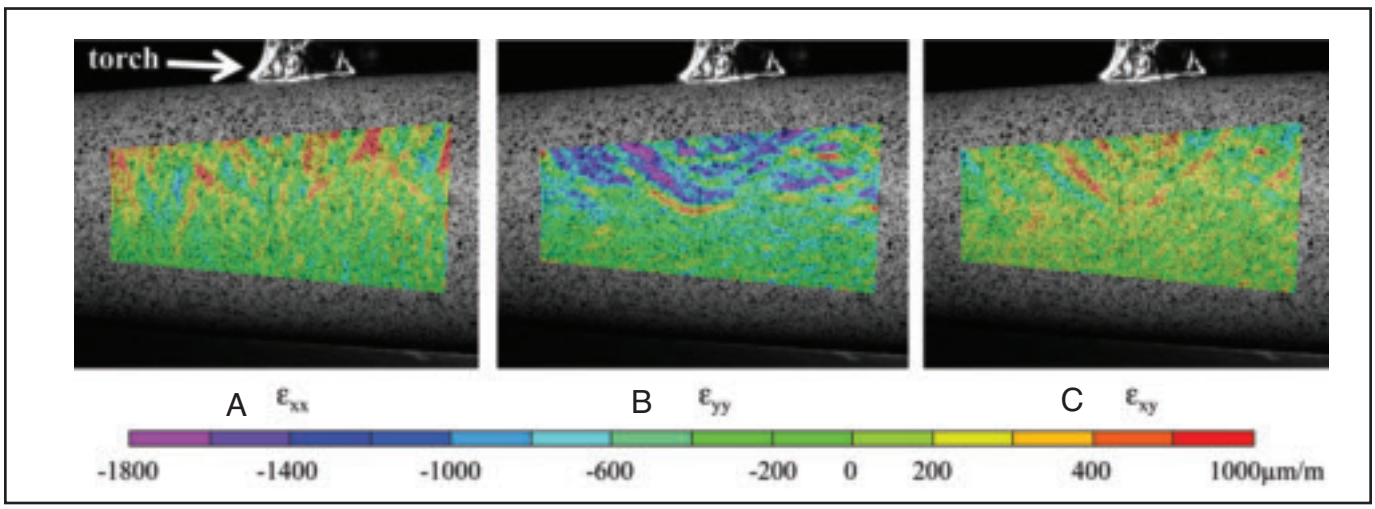

Fig. 4 — Full field strain map of the strain during the welding at t = 75 s. A — Longitudinal; B — hoop direction; C — shear strain. The torch is shielded by a tin foil.

size is applied, i.e., for a step size of 2 px, the subset is moved 2 px from its original position, which means that displacement results are not available for every pixel, but on a grid two times coarser than the pixel grid.

Next, the obtained displacements are smoothed via a so-called strain window (SW) method to reduce the impact of uncertainties and noise. This is a commonly adopted technique during the process of strain derivation (Ref. 18). In this step of the analysis, a plane is fit through the displacement values in the points around the center of the strain window (CSW) where displacements are available. This analytical approximation makes the calculation of the full-field strain information straightforward. In this research, a default strain window of 5 is used. This means that the displacement field is smoothed over an area of 5 × 5 displacement data points, or with a step size of 2 px, over an area of 8 × 8 px around the CSW.

Setup

The weld bead is put on the tube in a longitudinal direction, representing the closing bead that is laid in the real production process of the cold-rolled steel tube. Neither in the actual welding of the tube is filler material used, nor in this experimental setup. The tube is kept fixed, while the torch is moving on top of it — Fig. 1.

The torch is held perpendicular to the tube's surface by a ABB IRB1600 robot, allowing a constant torch travelling speed of 2 mm s^{-1} and a 2-mm arc length between the base metal and the tip of the electrode. The tungsten 2%-lanthaned electrode with a diameter of 1.6 mm has an extension of 1.4 mm out of the 7-mm-diameter cup. The shielding gas is pure argon with a flow of 10 L/min^{-1}. This setup yields a stable welding process, with a constant current of 38 A set and a voltage of 8 V measured over the beam. The weld bead has a length of 300 mm, assuring stable welding conditions in the middle 200 mm of the tube. To avoid overexposure on the images taken during the welding, the blazing light of the weld beam was shielded by a tin foil wrapped around the cup of the torch.

The SS304 stainless steel tube (chemical composition: 0.04%C; 0.4%Si; 1.28Mn, 0.03%P; 0.00%S; 18.2%Cr; 0.32%Mo; 7.63%Ni; 0.08%V; 0.003%Al; 0.55%Cu;

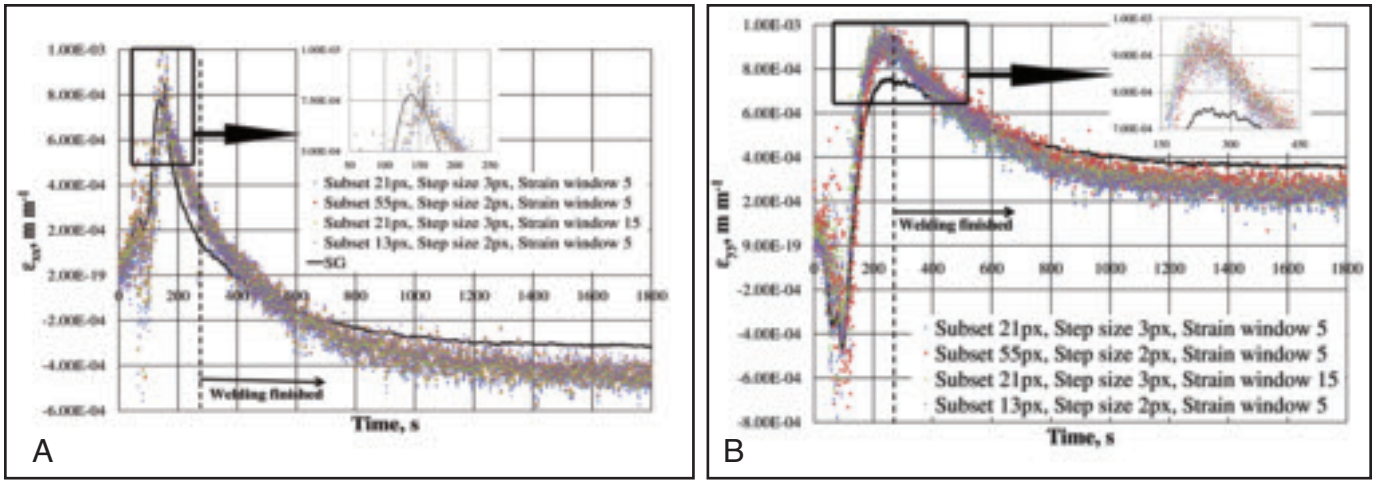

Fig. 5 — A — Strain evolution in SG// compared to DIC results (ε_{xx}) with different correlation parameters, torch in x-position of SG// at t = 90.5 s; B — strain evolution in SG+ compared to DIC results (ε_{yy}) with different correlation parameters, torch in x-position of SG// at t = 73 s.

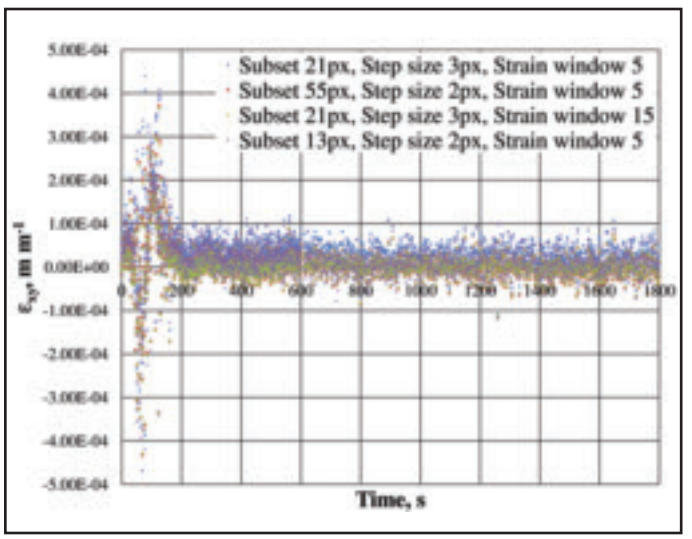

Fig. 6 — Shear strain evolution in the area of the tube corresponding to SG+.

0.004%Ti) under consideration has a diameter of 60 mm, a wall thickness of 1.5 mm, and a length of 400 mm. The tube is clamped at the bottom side with a massive steel bar of diameter 25 mm inside the tube, at both ends screwed to a steel support (a bar of 20 × 40 × 500 mm) — Fig. 1B.

At one side of the tube, in an area of about 40 × 200 mm, a uniform white paint layer is put on the tube. This paint is heat-resistant silicon resin type paint applied with an airbrush. On this white coat, a random speckle pattern is applied with black paint of the same type. The speckles have a maximum size of about 1 mm^2. Markers (black crosses) are integrated in this speckle pattern as a reference for the focus of the cameras — Fig. 2. These markers are drawn with a black, narrow pointed (0.2 mm) felt-tip pen. These markers are also used in the processing of the images for assigning a coordinate system. As displacements are known in all directions and over a certain area, strains can be calculated in different coordinate systems.

Two CCD cameras are focussed on the middle of the speckle pattern. These cameras are monochrome 12-bit cameras with a resolution of 1280 × 1024 px and are equipped with Schneider Kreuznach xenoplan 1.4/23 lenses. The cameras are positioned in the same horizontal plane as the axis of the tube and have an intermediate angle of 60 deg. The distance between the cameras and the tube is about 265 mm. For each test, the camera system is calibrated, yielding the intrinsic (focal length, image plane center location, distortion parameters of the lenses) and extrinsic (rotational and translational definition of the camera system) parameters of the camera setup. In this setup, one pixel has a physical dimension of about 0.072 mm. This dimension is approximate as the cameras are looking at the curved surface and are tilted from the surface normal. The focus of the cameras is at the position of 90 deg seen from the weld bead — Fig. 1. With this setup, the area of the tube that can be followed is 80 × 30 mm (the field of view is larger, but due to the curvature of the surface of the tube, not the whole speckle pattern is visible in the images — Fig. 2). Images are taken in two series: In the first 600 s of the experiment every 0.5 s an image is taken, and in the next 1200 s every second an image is taken, leading to a total of 2400 images from which the strain evolution can be calculated.

Five K-type thermocouples (TC) were installed on the side of the tube opposite to the speckle pattern. One SG (SG+) measures the hoop strain and one SG (SG//) measures the longitudinal strain at a position of 90 deg seen from the weld bead. As the position of the SG is symmetric to the speckle pattern from the point of the weld bead, a comparison between the strain measured with DIC and SG is possible. The thermocouples were necessary to compensate for spurious thermal strains in the SG (see next section). The position of the SG was chosen in an area where the temperatures are not too high for the glue (Z70, a cyanoacrylate adhesive), and the range in which the temperature compensation is known from the producer (up to 120°C). The gauges used in this setup were HBM 1-LY15-6/350A 350 Ω resistance strain gauges, have a measuring grid of 3 × 6 mm and are compensated for a material with a thermal expansion coefficient of α_{SG} = 16 µm m^{-1}°C^{-1}. The SG and TC signals are read out by a Spider 8 amplifier and processed with Catman software.

Strain gauges and thermocouples are disconnected from the amplifier during the start of the weld beam to avoid problems with heavy electrical fields initiated by the starting of the beam. Therefore, in the beginning of the experiments, there are no results of SG and TC.

Results

The strains measured with the SG have to be compensated for temperature effects, since apparent strains ε_a are measured when using strain gauges for strain measurement under varying temperature conditions (Ref. 19).

$$\varepsilon_a = \varepsilon_m + \varepsilon_s + (\alpha_m - \alpha_{SG}) \cdot \Delta\theta, \quad (1)$$

with ε_a the apparent strain, indicated by the amplifier; ε_m the strain triggered by the mechanical load (zero in these experiments); ε_s the apparent strain of the strain gauge without mechanical strain, known as a function of temperature for each strain gauge; α_m the linear coefficient of thermal expansion (CTE) of the measured object; α_{SG} the CTE of the strain gauge (in these experiments 16 µm $m^{-1}°C^{-1}$), and $\Delta\theta$ the temperature interval over which the strain is measured. The thermal strain in the object is defined as

$$\varepsilon_{th} = \alpha_m \cdot \Delta\theta \quad (2)$$

Combining formula 1 and 2 leads to the thermal strain at the SG position

$$\varepsilon_{th} = \varepsilon_a - \varepsilon_s + \alpha_{SG} \cdot \Delta\theta \quad (3)$$

The curve for temperature measurement is given in Fig. 3A, the uncorrected and corrected SG curve are given in Fig. 3B. The peak in the SG values at about 153 s is the reflection of the peak in the temperature curve, which is caused by switching off the torch.

The calculation of the DIC displacements and strains was performed with the commercial Vic3D software from Correlated Solutions. A full-field strain map is shown in Fig. 4. The resulting strain evolution during the welding and the cooling of the tube at corresponding positions and in the same direction as the SG are plotted in Fig. 5. A coordinate system with the x-axis through the three crosses on the horizontal line was assigned as the reference for the displacement and strain calculation. The strain obtained from SG// is therefore compared to the normal strain in the x-direction and the strain from SG+ to the normal strain in the y-direction.

As one pixel has a dimension of about 0.072 mm and the measuring grid of the SG is 3 × 6 mm^2, the strain obtained from a SG is in fact the average strain over this area, or in terms of DIC, the strain averaged over a surface area of 40 × 80 px. To compare the strains obtained with DIC and those with a SG, strains of all the CSW within the area of a SG were averaged and taken as the strain to compare with the SG results. This means that the strains plotted in Fig. 5 are averaged over a region of 40 × 80 px, corresponding to 800 CSW (as the step size in this example is 2 px).

As with the DIC method, subset, step, and strain window size are ought to cause the most influence on the found strain, these parameters were investigated. In Fig. 5, three subset sizes were investigated: 13 px (the smallest possible, related to the speckle size), 21 px (a medium size subset), and 55 px (a rather large subset size). To maximize the amount of information, the step size was chosen small: 2 or 3 px. The influence of the strain window was investigated for two sizes: 5 and 15. Results of different tests show similar strain results, both for temperature development, strain obtained from SG measurement, and strain from DIC calculation. The results for one test are published here.

Discussion

In formula 3, the two terms ε_s and $\Delta\theta$ can only be determined with knowledge of the temperature at the location of the SG. This emphasizes the importance of accurate temperature measurements in the neighborhood of the SG, which complicates the SG measurements.

From the results shown in Fig. 4, it can be concluded that the DIC results are insensitive to the investigated parameters. Although we would expect that a larger subset and a larger SW would reduce the noise on the data, this does not seem to be the case. This can be explained by the SW procedure, which already cancels the impact of the subset size, approving the efficiency of the SW procedure. The small impact of the SW can be explained by the very smooth displacement behavior in this application. Looking at Figs. 4–6, the DIC data are very noisy, but the strain evolution in the process is easily revealed in Figs. 5 and 6. Thus, it can be concluded that it is possible to measure the strain during a welding process with DIC and those results are, within the investigated range in this research, relatively insensitive to the correlation parameters. The noise on the data can be explained by the small displacements and small strains that we are trying to measure in these experiments. Generally, DIC is not considered for measuring strains below 1000 $\mu m\ m^{-1}$. When the deformations become larger, e.g., closer to the weld bead, the noise on the strain data should become smaller. Other possibilities for reducing the noise on the DIC data are using higher resolution CCD; reducing the field of view, which both might allow averaging over more points over the surface; or raise the number of frames taken per second, which might allow averaging over more points in time.

From Fig. 5, it is concluded that there is good agreement between the DIC results and the SG results. Although the SG allows a higher sampling rate than the cameras that are currently used in the measurements, the DIC measurements capture all the relevant strain peaks as well. More up-to-date cameras allow a higher sampling frequency (easily up to 30 frames per second). The difference between the strain calculated with the SG and DIC can be due to the temperature compensation of the SG and creep effects in the glue of the SG.

In Fig. 6, the in-plane shear strains obtained with DIC are shown. As can be inferred, these are zero during the largest part of the experiment. This reveals the principal strain directions: the hoop and the longitudinal directions. If we wanted to discover this with strain gauges, it would have taken a strain gauge rosette consisting of three strain gauges. This means also that at that point we are measuring the principal strains in the material during the cooling phase with the SG. From preliminary FE simulations, it is known that the shear strain in the cooling phase of the welding is zero. Comparing the shear strain from DIC and FE leads to the conclusion that 95% of the DIC results have a noise smaller than 70 μm/m.

Smaller averaging areas hamper a clear interpretation of the results due to the larger noise and increasing influence of the subset and strain window size on the strain curve. Nevertheless, more detailed information about the strain state in the material can be retrieved than possible with resistance strain gauges.

Compared to other transient deformation measurement techniques, DIC has the advantages that it is a contactless method, does not require temperature compensation, has a rather simple setup, is robust to vibrations, allows to observe the strains over a whole field, and it is possible to measure in all the visible parts of the welded construction even close to the weld. Good lighting conditions are needed, including a shielding of the weld beam to avoid overexposure on the images as the torch is passing.

As this technique is still evolving, better results can be expected in the near future. Points of improvement are the lenses on the camera that allow for a better zoom (but smaller field of view), the use of high-speed cameras that allow averaging in the time domain and application of this technique to faster welding processes.

Conclusions

The main conclusion of this contribution is that in the configuration as described here, it is possible to obtain the strain field with DIC. As it is difficult to obtain a reference strain measurement, the strains calculated with DIC are compared to SG measurements and show good agreement. The strains measured with SG are sensitive

to temperature compensation, implicating an accurate temperature measurement in the neighborhood of the SG. For validation of finite element simulations, transient deformation measurements are preferred as these allow validating the simulation of the process as a whole and not just the final stress/strain state. For the case under investigation, i.e., a tube in which we want to know the strain evolution during the welding process, DIC is a method preferred over other measuring techniques. With DIC we obtain the strain evolution over a substantial part of the surface, which allows a validation of the FEA result over a large domain, both in space (2400 mm^2) and time (from the weld start till complete cool down). It is possible to measure the strains without knowledge of the temperature (as DIC requires no temperature compensation) and in a hot region of the tube, close to the weld bead, as the cameras that capture the images make no contact with the tube.

The results of the measurement with the DIC technique as explained in this contribution give an outlook on using this method as a validation tool for FE simulations of welding processes on different geometries. For realistic comparison of the strain evolution, however, the residual stresses already present in the construction under investigation (i.e., a tube with residual stresses due to rolling and preliminary welding) have to be known. Alternatively, the experiment should be performed on an initially stress free sample.

Acknowledgments

The authors would like to thank R. De Coster for the help with controlling the robot and R. Van Hecke for the help with the setup of the welding equipment and the practical tips.

References

1. Lindgren, L. 2001. *Journal of Thermal Stresses* 24: 305–334.

2. Muramatsu, Y., Kuroda, S., and Shiga, C. 2003. *Welding International* 17(8): 615–623.

3. Mikami, Y., Mochizuki, M., and Toyoda, M. *Mathematical Modelling of Weld Phenomena 8*, eds. H. Cerjak, H. Bhadeshia, and E. Kozeschnik. Technische Universität Graz, pp. 981–1001.

4. Schwenk, C., Rethmeier, M., and Weiss, D. *Mathematical Modelling of Weld Phenomena 8*, eds. H. Cerjak, H. Bhadeshia, and E. Kozeschnik. Technische Universität Graz, pp. 835–846.

5. Van der Aa, E., Thiessen, R., Murugaiyan, A., Hermans, M., Sietsma, J., and Richardson, I. *Mathematical Modelling of Weld Phenomena 8*, eds. H. Cerjak, H. Bhadeshia, and E. Kozeschnik. Technische Universität Graz, pp. 387–408.

6. Van der Aa, E., Hermans, M., and Richardson, I. *Mathematical Modelling of Weld Phenomena 8*, eds. H. Cerjak, H. Bhadeshia, and E. Kozeschnik. Technische Universität Graz, pp. 1053–1072.

7. Courtin, S., and Gilles, P. *Mathematical Modelling of Weld Phenomena 8,* eds. H. Cerjak, H. Bhadeshia, and E. Kozeschnik.Technische Universität Graz, pp. 603–626.

8. DeStycker, M., Schueremans, L., Van Paepegem, W., and Debruyne, D. *Optics and Lasers in Engineering.* in press.

9. Lyons, J., Liu, J., and Sutton, M.1996. *Experimental Mechanics* 36(1): 64–70.

10. Pan, B., Wu, D., and Xia, Y. 2010. *Optics and Lasers in Engineering* 48(9): 841–848.

11. Cooreman, S., Lecompte, D., Vantomme, J., Sol, H., and Debruyne, D. 2008. *Experimental Mechanics* 48: 421–433.

12. Lecompte, D., Cooreman, S., Coppieters, S., Vantomme, J., Sol, H., and Debruyne, D. 2009. *European Journal of Computational Mechanics* 18: 393–418.

13. Van Paepegem, W., Shulev, A., Roussev, I., De Pauw, S., Degrieck, J., and Sainov, V. 2009. *Optics and Lasers in Engineering* 47: 390–397.

14. Ivanov, D., Ivanov, S., Lomov, S., and Verpoest, I. 2009. *Optics and Lasers in Engineering* 47: 360–370.

15. Sutton, M., Orteu, J., and Schreier, H. 2009. *Image Correlation for Shape, Motion and Deformation Measurements.* Springer, New York, doi: 10.1007/978-0-387-78747-3.

16. Lava, P., Cooreman, S., Coppieters, S., De Strycker, M., and Debruyne, D. 2009. *Optics and Lasers in Engineering* 47: 747–753.

17. Schreier, H., Braasch, J., and Sutton, M. 2000. *Optical Engineering* 39: 2915–2921.

18. Lava, P., Cooreman, S., and Debruyne, D. 2010. *Optics and Lasers in Engineering* 48: 457–468.

19. HBM: Experimental stress analysis — correcting thermally induced strain during strain gauge measurements, can strain gauges be used to determine the thermal coefficient of linear expansion of a given material?